Preexisting tissue mechanical hypertension at adherens junctions disrupts apoptotic extrusion in epithelia

Zoya Mann[a], Fayth Lim[a], Suzie Verma[a], Bageshri N. Nanavati[a], Julie M. Davies[b], Jakob Begun[b,c], Edna C. Hardeman[d], Peter W. Gunning[d], Deepa Subramanyam[e], Alpha S. Yap[a,*], and Kinga Duszyc[a,*]

[a]Division of Cell and Developmental Biology, Institute for Molecular Bioscience, The University of Queensland, Brisbane, Australia 4072; [b]Mater Research – The University of Queensland, Woolloongabba, Queensland, Australia 4102; [c]Department of Gastroenterology, Mater Hospital Brisbane, South Brisbane, Australia 4101; [d]School of Biomedical Sciences, Faculty of Medicine and Health, Univeristy of New South Wales Sydney, New South Wales, Australia 2052; [e]National Centre for Cell Science, Savitribai Phule Pune University, Pune 411007, India

ABSTRACT **Apical extrusion is a tissue-intrinsic process that allows epithelia to eliminate unfit or surplus cells. This is exemplified by the early extrusion of apoptotic cells, which is critical to maintain the epithelial barrier and prevent inflammation. Apoptotic extrusion is an active mechanical process, which involves mechanotransduction between apoptotic cells and their neighbors, as well as local changes in tissue mechanics. Here we report that the preexisting mechanical tension at adherens junctions (AJs) conditions the efficacy of apoptotic extrusion. Specifically, increasing baseline mechanical tension by overexpression of a phosphomimetic Myosin II regulatory light chain (MRLC) compromises apoptotic extrusion. This occurs when tension is increased in either the apoptotic cell or its surrounding epithelium. Further, we find that the proinflammatory cytokine, TNFα, stimulates Myosin II and increases baseline AJ tension to disrupt apical extrusion, causing apoptotic cells to be retained in monolayers. Importantly, reversal of mechanical tension with an inhibitory MRLC mutant or tropomyosin inhibitors is sufficient to restore apoptotic extrusion in TNFα-treated monolayers. Together, these findings demonstrate that baseline levels of tissue tension are important determinants of apoptotic extrusion, which can potentially be coopted by pathogenetic factors to disrupt the homeostatic response of epithelia to apoptosis.**

SIGNIFICANCE STATEMENT

- Apical extrusion is a mechanically active process that allows epithelia to eliminate apoptotic cells. Here we report that upregulating the prevailing mechanical tension at adherens junctions compromises apical extrusion, causing apoptotic cells to be retained in epithelial monolayers.
- We upregulated mechanical tension by expressing a phosphomimetic Myosin regulatory light chain mutant and also with TNFα. Importantly, apoptotic extrusion could be restored to TNFα-treated monolayers by reducing mechanical tension, using mutant MRLC or tropomyosin inhibitor drugs.
- Baseline tissue tension is a crucial regulator of apoptotic extrusion. Inflammation may inhibit extrusion, causing apoptotic cells to be retained, by increasing epithelial mechanical tension.

Monitoring Editor
Jody Rosenblatt
King's College London

Received: Sep 5, 2023
Revised: Oct 13, 2023
Accepted: Oct 20, 2023

This article was published online ahead of print in MBoC in Press (http://www.molbiolcell.org/cgi/doi/10.1091/mbc.E23-08-0337) on October 30, 2023.

Conflicts of Interest: E.C. Hardeman reports receiving a commercial research grant from and has ownership interest (including patents) in TroBio Therapeutics P.W. Gunning reports receiving other commercial research support from and has ownership interest (including patents) in TroBio Therapeutics. A.S. Yap is an Associate Editor of MBoC. No potential conflicts of interest were disclosed by the other authors.

*Address correspondence to: Kinga Duszyc (k.duszyc@imb.uq.edu.au); Alpha S. Yap (a.yap@imb.uq.edu.au).

Abbreviations used: Caco-2, cancer coli-2 epithelial cells; CTCF, corrected total cell fluorescence; EGTA, ethylene glycol tetraacetic acid; GFP, green fluorescent protein; IFN-γ, Interferon-γ; IL-8, Interleukin-8; MLCK, Myosin Light Chain Kinase; MRLC-AA, Myosin Regulatory Light Chain-Ala-18,Ala-19; MRLC-DD, Myosin Regulatory Light Chain-Asp-18,Asp-19; MRLC, Myosin regulatory light chain; PIPES, piperazine-1,4-bis(2-ethanesulfonic acid); pMRLC, phospho-myosin regulatory light chain; SEM, standard error of mean; TNFR1, tumor necrosis factor receptor-1; TNFα, tumor necrosis factor α; TPMi, tropomyosin Inhibitor.

INTRODUCTION

Epithelia constitute primary body barriers that protect their underlying tissues from environmental dangers. Epithelial cells are physically coupled to one another, forming tissue layers that can respond to diverse stimuli in a well-coordinated manner (Lecuit and Yap, 2015). Adherens junctions (AJs) are specialized epithelial cell–cell junctions, built upon classical cadherin adhesion complexes that physically couple to the contractile actomyosin network. This cytoskeletal association can generate mechanical tension in the junctions, creating the potential for AJs to form a tensile network that connects cells together in epithelial monolayers (Charras and Yap, 2018). Dynamic patterns of change in AJ tension influence cell–cell rearrangements during morphogenesis in the embryo (Heer and Martin, 2017). They also participate in homeostasis during postdevelopmental life, as exemplified by the epithelial response to apoptosis (Lubkov and Bar-Sagi, 2014; Michael *et al.*, 2016; Duszyc *et al.*, 2021a).

Epithelial integrity is constantly challenged by environmental stresses that can cause apoptosis. Extrusion constitutes a first-line response to the apoptotic challenge that robustly eliminates dying cells in a manner of minutes (Rosenblatt *et al.*, 2001; Michael *et al.*, 2016; Duszyc *et al.*, 2021a). If the extrusion response fails, retained apoptotic cells can disrupt the functional epithelial barrier and provoke proinflammatory responses from neighboring epithelial cells (Duszyc *et al.*, 2023). Successful extrusion involves a complex series of mechanical changes in the apoptotic cells and their proximal neighbors (Supplemental Figure S1A; Teo *et al.*, 2020b). In one set of changes, hypercontractility of apoptotic cells stimulates the adjacent cells to assemble a contractile cortex at their interface with the apoptotic cells (Andrade and Rosenblatt, 2011; Lubkov and Bar-Sagi, 2014; Duszyc *et al.*, 2021a; Atieh *et al.*, 2021). Contraction of this cortical network drives the physical expulsion of the dying cells. In parallel, AJs in neighbour cells that are oriented tangential to the apoptotic cell undergo mechanical relaxation (Teo *et al.*, 2020b). This facilitates apoptotic extrusion, and itself appears to be a response to transient early relaxation in the acutely injured cells (Teo *et al.*, 2020b). These complex local patterns of mechanical change therefore appear to reflect multiple mechanotransduction pathways that mediate communication from apoptotic cells to their neighbors.

The dynamic changes in AJ tension associated with apoptotic extrusion occur upon a preexisting or baseline pattern of mechanical junctional tension (Teo *et al.*, 2020b). This raises the interesting question of whether aberrant change in baseline AJ tension can affect the efficacy of apoptotic extrusion. Recently, we reported that an increase in baseline AJ tension (mechanical hypertension, for short) compromised the ability of epithelial monolayers to eliminate oncogene-expressing cells by apical extrusion (Teo *et al.*, 2020a). Additionally, increased levels of junctional Myosin II were shown to have an inhibitory effect on basal cell delamination in *Drosophila* notum (Curran *et al.*, 2017). Whether this may apply for apoptotic apical extrusion is not yet known. We now report that increasing preexisting AJ tension using a phosphomimetic Myosin regulatory light chain (MRLC) mutant (MRLC-DD) decreases the ability of epithelial monolayers to execute apoptotic extrusion. Further, we show that the inflammatory cytokine, TNFα, also increases baseline AJ tension, and this compromises the elimination of apoptotic cells by apical extrusion. This highlights how baseline tissue tension regulates apical extrusion and suggests that changes in preexisting tension may cause homeostasis to be compromised in disease.

RESULTS AND DISCUSSION

MRLC-DD increases adherens junction tension in Caco-2 monolayers

To assess the potential implications of altered epithelial mechanics, we established a Caco-2 line stably expressing a phosphomimetic mutant of MRLC-DD (Supplemental Figure S1, B and C). As actomyosin is the major contributor to cellular force generation, MRLC-DD is predicted to enhance actomyosin activity, resulting in increased intercellular junctional tension.

To characterize the impact of MRLC-DD expression on AJ tension, we first examined the cellular localization of nonmuscle Myosin IIA and IIB, as well as the F-actin network. Levels of nonmuscle Myosin IIA and Myosin IIB (Figure 1, A–C) and F-actin (Figure 1, D–E) were increased at AJ in the MRLC-DD-expressing monolayer when compared with control GFP-expressing cells. The increase in junctional Myosin IIA and IIB was not associated with overall changes in expression levels of these proteins (Supplemental Figure S1, D–G). This suggested that contractile tension might be increased at AJ in MRLC-DD–expressing cells.

To pursue this further, we applied more direct approaches to evaluate potential changes in AJ tension. First, we tested whether MRLC-DD affects junctional tension by assessing the recoil of junctions (visualized by mCherry tagged endogenous ZO-1) after they were cut with a 2-photon laser beam (Liang *et al.*, 2016). Following laser ablation, junctions in the GFP-expressing control cells exhibited a prompt recoil (Supplemental Figure S1, H–J), indicating that they were tensile in steady-state Caco-2 monolayers. Importantly, the recoil (Supplemental Figure S1, H–J) and the initial velocity of the recoil (Figure 1F) were significantly increased in the MRLC-DD-expressing cells, consistent with increased junctional tension. To complement this experiment, we asked whether we could detect tension-associated changes at a molecular level. Specifically, we focused on cadherin-associated α-catenin, which is reported to undergo conformational changes upon application of tension to the E-cadherin complex (Yonemura *et al.*, 2010; Noordstra *et al.*, 2023). Here, we utilized an antibody (α-18 mAb), which detects a tension-exposed epitope in the central, M-domain of α-catenin (Nagafuchi and Tsukita, 1994). To correct for heterogeneity in staining intensity among samples, we used the ratio of α-18 to total α-catenin as a readout of molecular-level tension. MRLC-DD-expressing cells displayed a significantly higher ratio of junctional α-18/total α-catenin than the control cells (Figure 1, G and H). We corroborated this by measuring junctional levels of vinculin, which is recruited to α-catenin under tension (Yonemura *et al.*, 2010; Yao *et al.*, 2014). Consistent with our earlier results, junctional vinculin, corrected for α-catenin levels, was increased by expression of MRLC-DD (Figure 1, I and J). Taken together, our observations confirmed that junctional tension was elevated by expression of the MRLC-DD transgene in Caco-2 monolayers, which is consistent with previous reports.

Elevated baseline adherens junctional tension disrupts apoptotic extrusion

Then, we asked whether global increase in baseline junctional tension could affect the ability of epithelia to expel apoptotic cells. To test this idea, we treated control and MRLC-DD–expressing monolayers with the topoisomerase II inhibitor etoposide, which is commonly used to induce sporadic apoptosis in epithelial cell culture models (Andrade and Rosenblatt, 2011; Michael *et al.*, 2016; Teo *et al.*, 2020b; Duszyc *et al.*, 2021a). Strikingly, while control cells were able to robustly expel cleaved caspase-3 positive apoptotic cells (Figure 2, A and B), the MRLC-DD cells were significantly less efficient at eliciting extrusion (Figure 2, A and B). This drop in the

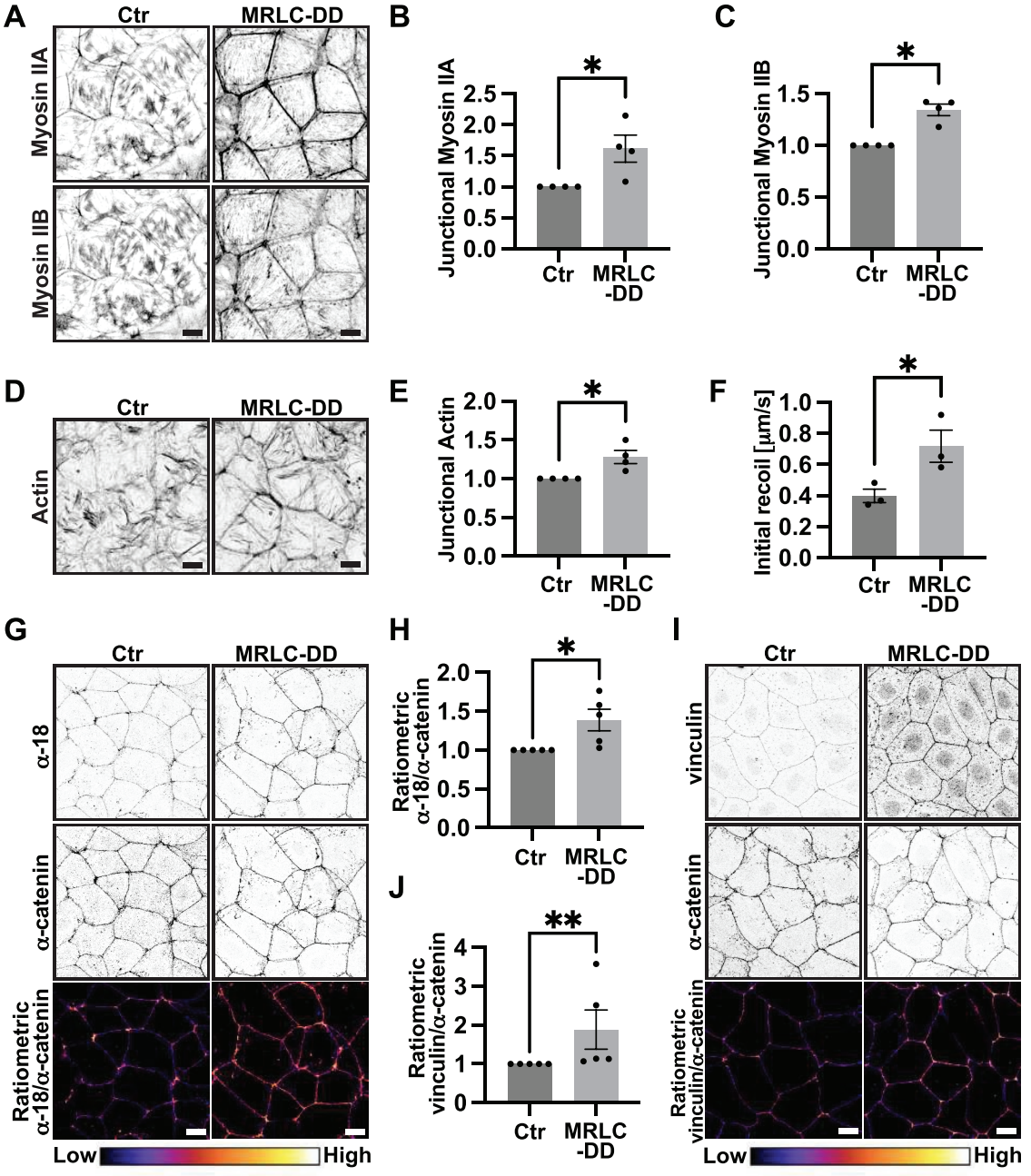

FIGURE 1: MRLC-DD increases junctional tension in Caco-2 monolayers. (A–C) Representative images (A) and quantification of Myosin IIA (B) and IIB (C) junctional localization in control and MRLC-DD cell lines. (D and E) Representative images (D) and quantification (E) of actin junctional localization in control and MRLC-DD cell lines. (F) Initial recoil of ablated junctions in control and MRLC-DD cell lines. (G and H) Representative images (G) and quantification (H) of junctional localization of α-catenin in open conformation (α-18) and total α-catenin in control and MRLC-DD cell lines. Ratiometric images represent junctional intensity of α-18 divided by junctional intensity of total α-catenin. (I and J) Representative images (I) and quantification (J) of junctional localization of vinculin and α-catenin in control and MRLC-DD cell lines. Ratiometric images represent junctional intensity of vinculin divided by junctional intensity of total α-catenin. Scale bars: 15 µm. XY panels are maximum projection views of all z-stacks. All data are means ± SEM; *$p < 0.05$, **$p < 0.01$, calculated from $n \geq 3$ independent experiments analyzed with unpaired Student's *t* test.

extrusion efficiency was not caused by a difference in apoptotic rates in the MRLC-DD monolayers compared with the controls (Supplemental Figure S2, A–C). We then induced apoptosis by microirradiating nuclei with a 2-photon laser (Teo *et al.*, 2020b; Duszyc *et al.*, 2021a,b), which provided tight temporal control of injury to monitor the extrusion process with high spatiotemporal resolution (Figure 2C). To visualize the behaviour of the neighbour cells we performed these experiments in control and MRLC-DD-expressing cell monolayers in which endogenous ZO-1 was tagged with mCherry by CRISPR/Cas9 genome editing (Duszyc *et al.*, 2023). We observed that AnnexinV–positive apoptotic cells were successfully extruded apically out of the control monolayer, typically within less than 60 min following laser injury (Figure 2, C–E). This was associated with elongation of the immediate neighbors of the apoptotic

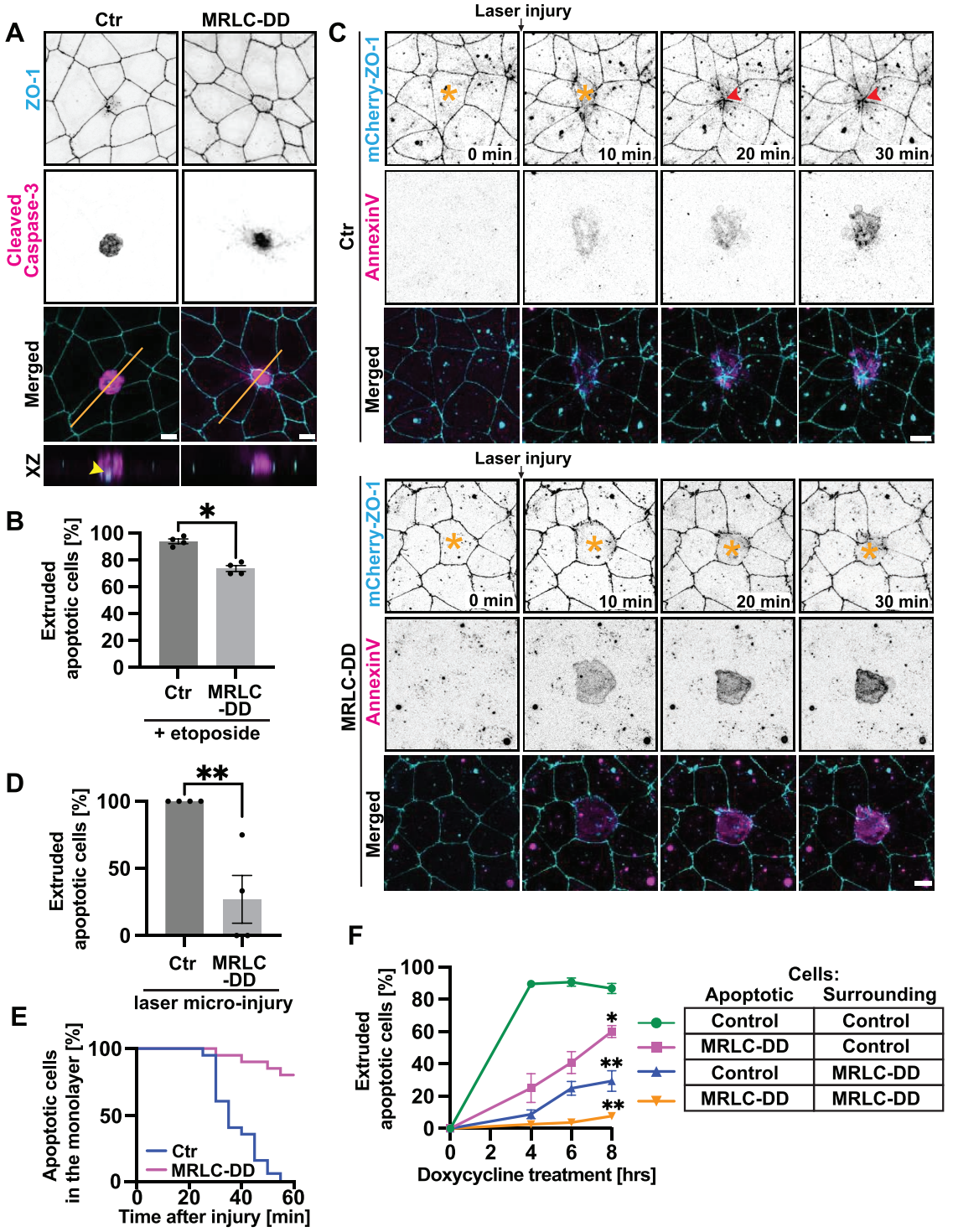

FIGURE 2: Increased baseline junctional tension compromises apoptotic extrusion. (A and B) Representative images (A) and quantification (B) of extrusion efficiency in etoposide treated (500 μM, 8 h) control and MRLC-DD cell lines. Orange lines- location of the XZ views; arrowhead - junctional closure underneath extruded apoptotic (cleaved-caspase positive) cell. (C–E) Selected frames from live imaging of 2-photon laser-mediated apoptosis in control and MRLC-DD cell lines (C). Apoptosis was confirmed by positive AnnexinV staining. Asterisks– apoptotic cells in the monolayers; arrowheads – junctional closure underneath extruded apoptotic cell. (D) Quantification of efficiency of apoptotic extrusion in control and MRLC-DD cell lines. Extrusion was classified as successful if apoptotic cells were expelled from the monolayers within 60 min after the 2-photon laser microinjury. (E) Representation of time [min] apoptotic cells were present within the monolayer before extrusion was completed. (F) Quantification of extrusion efficiency of PUMA-expressing apoptotic cells at 4, 6, and 8 h of doxycycline (2 μg/ml) treatment in mixed cell cultures. Scale bars: 15 μm. XY panels are maximum projection views of all z-stacks. All data are means ± SEM; *$p < 0.05$, **$p < 0.01$, calculated from $n \geq 3$ independent experiments analyzed with unpaired Student's t test (B and D) or two-way ANOVA (F).

cells, culminating in formation of a rosette-like pattern underneath the apically extruded cells (Figure 2C). In contrast, MRLC-DD-expressing monolayers commonly failed to extrude the dying cells (Figure 2, C–E). Instead, AnnexinV-positive apoptotic cells persisted within the epithelial layers for over 60 min (Figure 2E). Together, these observations indicated that a global increase of baseline AJ tension can impede the epithelial-intrinsic ability of monolayers to extrude apoptotic cells.

These results complement our earlier report that enhanced tissue tension compromises the efficiency of oncogenic extrusion (Teo *et al.*, 2020a). Of note, oncogenic extrusion was inhibited when tension was upregulated exclusively in the surrounding epithelium, rather than in the oncogene-expressing cell itself. We then asked whether this holds true for apoptotic extrusion. For this, we employed a cell-mixing protocol that allowed us to independently increase contractile tension in these different cell populations (Supplemental Figure S2D). To induce apoptosis, we used the Tet-on system to express PUMA, a BH3-only protein that has been reported to robustly elicit cell death in epithelial cells (Duszyc *et al.*, 2021a; Bonfim-Melo *et al.*, 2022). First, we generated a stable cell line expressing $PUMA^{Tet\text{-}on}$ that was later transduced with a lentivirus carrying either MRLC-DD or a control soluble GFP transgene ($MRLC\text{-}DD^{PUMA}$ and $Control^{PUMA}$, respectively; Supplemental Figure S2D). Then, we mixed the $MRLC\text{-}DD^{PUMA}$ or $Control^{PUMA}$ cells with control or MRLC-DD cells in a 1:100 ratio, so that small clusters of PUMA-expressing cells (typically <2–4) were surrounded by nonapoptotic cells (Supplemental Figure S2D). The mixed cultures were grown to confluency, and expression of PUMA was induced with doxycycline. As expected, $Control^{PUMA}$ cells were efficiently extruded by surrounding control neighbors (Figure 2F; Supplemental Figure S2E), while hypertensile $MRLC\text{-}DD^{PUMA}$ cells were retained within the equally tensile MRLC-DD neighboring epithelium (Figure 2F; Supplemental Figure S2E).

In contrast, the rates of extrusion were significantly decreased when preexisting tension was increased in either the surrounding epithelium or in the apoptotic cells themselves (Figure 2F; Supplemental Figure S2E). Increasing mechanical tension in these different cell populations therefore appeared to independently compromise apoptotic extrusion. The reason for this remains to be elucidated. One possibility for the surrounding epithelium is that mechanical hypertension prevents neighboring cells from relaxing their orthogonal junctions (Supplemental Figure S1A) sufficiently to elongate and mediate extrusion (Teo *et al.*, 2020b). From the perspective of the cells that are targeted for apoptosis, early apoptotic cells were reported to release tension before they become hypercontractile. This initial relaxation of apoptotic cells appeared to generate a signal for neighbour cells to elongate their orthogonal junctions (Teo *et al.*, 2020b). Increasing preexisting contractility in apoptotic cells may then prevent them from generating a sufficient signal to engage elongation by their neighbors. These are interesting questions for future research.

TNFα upregulates junctional tension

Can AJ hypertension and retention of apoptotic cells occur in a pathophysiological context? To address this question, we focused on TNFα, a key proinflammatory cytokine upregulated in many inflammatory and autoimmune diseases, even when they are in clinical remission (Bradley, 2008; Ruder *et al.*, 2019; Jang *et al.*, 2021). Importantly, TNFα has been previously reported to transcriptionally upregulate Myosin Light Chain Kinase (MLCK), which can directly activate nonmuscle Myosin II (Ma *et al.*, 2005; Graham *et al.*, 2006). Therefore, we tested whether treatment of Caco-2 cells with TNFα affects AJ tension.

We found that TNFα-treated cells displayed more junctional nonmuscle Myosin IIA than untreated control cells (Figure 3, A and B). Also, the junctional pool of phosphorylated MRLC (pMRLC) was significantly increased by TNFα (Figure 3, C and D). This was accompanied by an increase in baseline AJ tension, as measured by ratiometric α-18 mAb/total α-catenin imaging (Figure 3, E and F). Additionally, both the recoil (Figure 3G; Supplemental Figure S3, A and B) and the initial speed of junctional recoil (Figure 3H) were enhanced in TNFα-treated monolayers. Together, the results indicate that stimulation of nonmuscle Myosin II by TNFα increases the mechanical tension in AJ.

TNFα perturbs apoptotic extrusion

Then, we asked whether induction of mechanical hypertension by TNFα affected the ability of epithelia to eliminate apoptotic cells by apical extrusion. To test this, we induced etoposide-mediated apoptosis in control and TNFα-treated cellular monolayers and quantified the percentage of apoptotic cells that were successfully extruded (Figure 4A; Supplemental Figure S4A). Whilst control cells robustly expelled almost 100% of AnnexinV-positive apoptotic cells, TNFα treatment decreased the extrusion efficiency to less than 50% (Figure 4A; Supplemental Figure S4A). We considered the possibility that the increased number of retained apoptotic cells we saw was due to enhanced cell mortality, as TNFα TNFR1 receptor is capable of inducing apoptosis (Micheau and Tschopp, 2003). To address this, we live-imaged TNFα-treated and control cell cultures. However, we did not detect a significant difference in the number of cells that underwent apoptosis in these two groups (Supplemental Figure S4B). As expected, etoposide increased the number of apoptotic cells detected during live-imaging, but the incidence of apoptosis was comparable between control and TNFα- treated monolayers (Supplemental Figure S4B). Consistent with this, we did not detect cleaved caspase-3 bands in immunoblots from control or TNFα-treated cells (Supplemental Figure S4, C and D), and the intensity of the bands was comparable in these two groups upon etoposide treatment (Supplemental Figure S4, C and D). Therefore, we reasoned that TNFα treatment did not stimulate apoptosis or sensitize cells to etoposide-induced cell death in our system.

We inferred instead that TNFα treatment perturbed extrusion of apoptotic cells. We tested this directly by inducing apoptosis with 2-photon nuclear microirradiation. In line with our previous observations, control monolayers expelled apoptotic cells typically within 30 min postinjury (Figure 4, B and C). In contrast, TNFα-treated cells were frequently unable to extrude apoptotic cells even 60 min postinjury, leading to prolonged retention of cell corpses within the epithelial layers (Figure 4, B–D). Together, this reinforced the notion that TNFα perturbs the epithelial-intrinsic ability to extrude apoptotic cells.

Correction of mechanical hypertension rescues apoptotic extrusion in TNFα-treated monolayers

As TNFα is known to cause diverse cellular effects (Tracey and Cerami, 1994; Leppkes *et al.*, 2014; Gough and Myles, 2020), we then asked whether the disruption of apoptotic extrusion in TNFα-treated monolayers was indeed caused by mechanical hypertension. For this we expressed a phosphodeficient mutant of MRLC (MRLC-AA) to reduce AJ tension in TNFα-treated monolayers. We confirmed that MLRC-AA reversed the enhanced baseline junctional tension caused by TNFα, as measured by ratiometric α-18 mAb/total α-catenin immunostaining (Figure 5, A and B). Importantly, we found that MRLC-AA significantly increased the percentage of apoptotic cells that were apically expelled from TNFα-treated epithelial monolayers

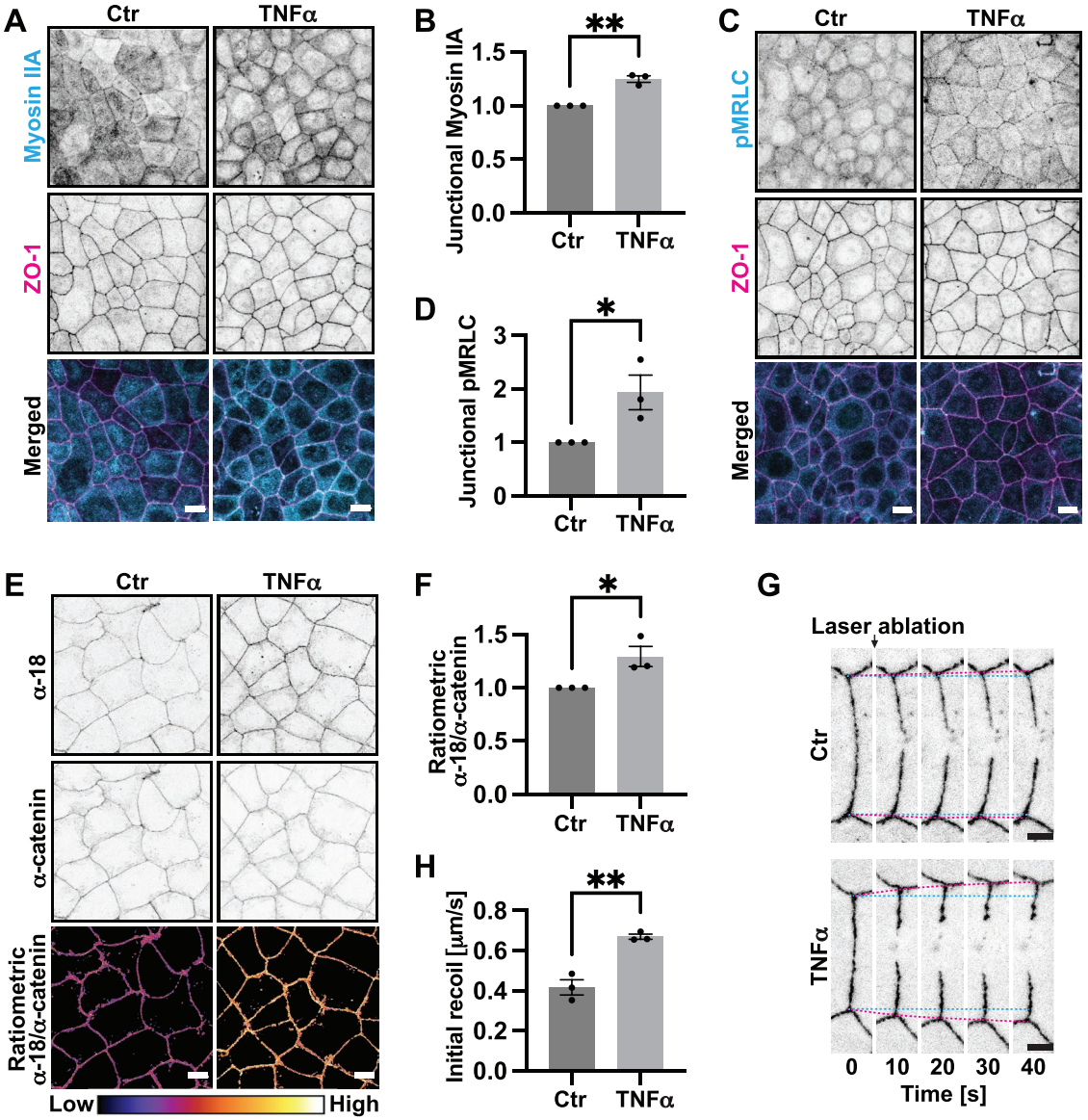

FIGURE 3: TNFα upregulates junctional tension. (A and B) Representative images (A) and quantification (B) of Myosin IIA junctional localization in control and TNFα-treated cell lines. (C and D) Representative images (C) and quantification (D) of pMRLC junctional localization in control and TNFα-treated cell lines. (E and F) Representative images (E) and quantification (F) of junctional localization of α-catenin in open conformation (α-18) and total α-catenin in control and TNFα-treated cell lines. Ratiometric images represent junctional intensity of α-18 divided by junctional intensity of total α-catenin. (G and H) Selected frames (G) from live imaging of 2-photon laser-mediated junction ablation followed by junctional recoil in control and TNFα-treated cells. Calculated speed of initial recoil (H) of ablated junctions in control and TNFα-treated cells. Scale bars: 15 µm. XY panels are maximum projection views of all z-stacks. All data are means ± SEM; *$p < 0.05$, **$p < 0.01$, calculated from $n \geq 3$ independent experiments analyzed with unpaired Student's *t* test.

(Figure 5, C and D). This implied that correcting junctional hypertension could restore apoptotic extrusion to TNFα- treated monolayers.

As an independent test of this idea, we used the structurally distinct tropomyosin inhibitors (TPMi) ATM1001 and ATM3507 (Currier *et al.*, 2017; Kee *et al.*, 2018) to reverse AJ hypertension. Tropomyosin supports actomyosin to generate contractile tension at AJs. Specifically, tropomyosin Tpm3.1 was shown to enhance Myosin IIA ATP turnover kinetics (Reindl *et al.*, 2022). Additionally, Actin-Myosin IIA filaments lacking Tpm3.1/Tpm3.2 provide only weak cortical tension (Wang *et al.*, 2023) and drug inhibition or depletion of Tpm3.1/Tpm3.2 can decrease junctional epithelial tension (Caldwell *et al.*, 2014). We found that treatment with either ATM1001 or ATM3507 reversed AJ hypertension (Figure 5, E and F) and increased the percentage of apoptotic cells that were extruded from the TNFα-treated monolayers (Figure 5, G and H). Therefore, reversal of mechanical hypertension can significantly enhance the ability of Caco-2 monolayers to expel apoptotic cells despite the continuous presence of TNFα. However, the extrusion efficiency was not returned to the levels observed in control monolayers (Figures 2, B and D and 4, A and D), suggesting that other effects of TNFα might also affect extrusion. Nevertheless, our results identify AJ mechanical hypertension as a significant factor that allows TNFα to perturb apoptotic extrusion.

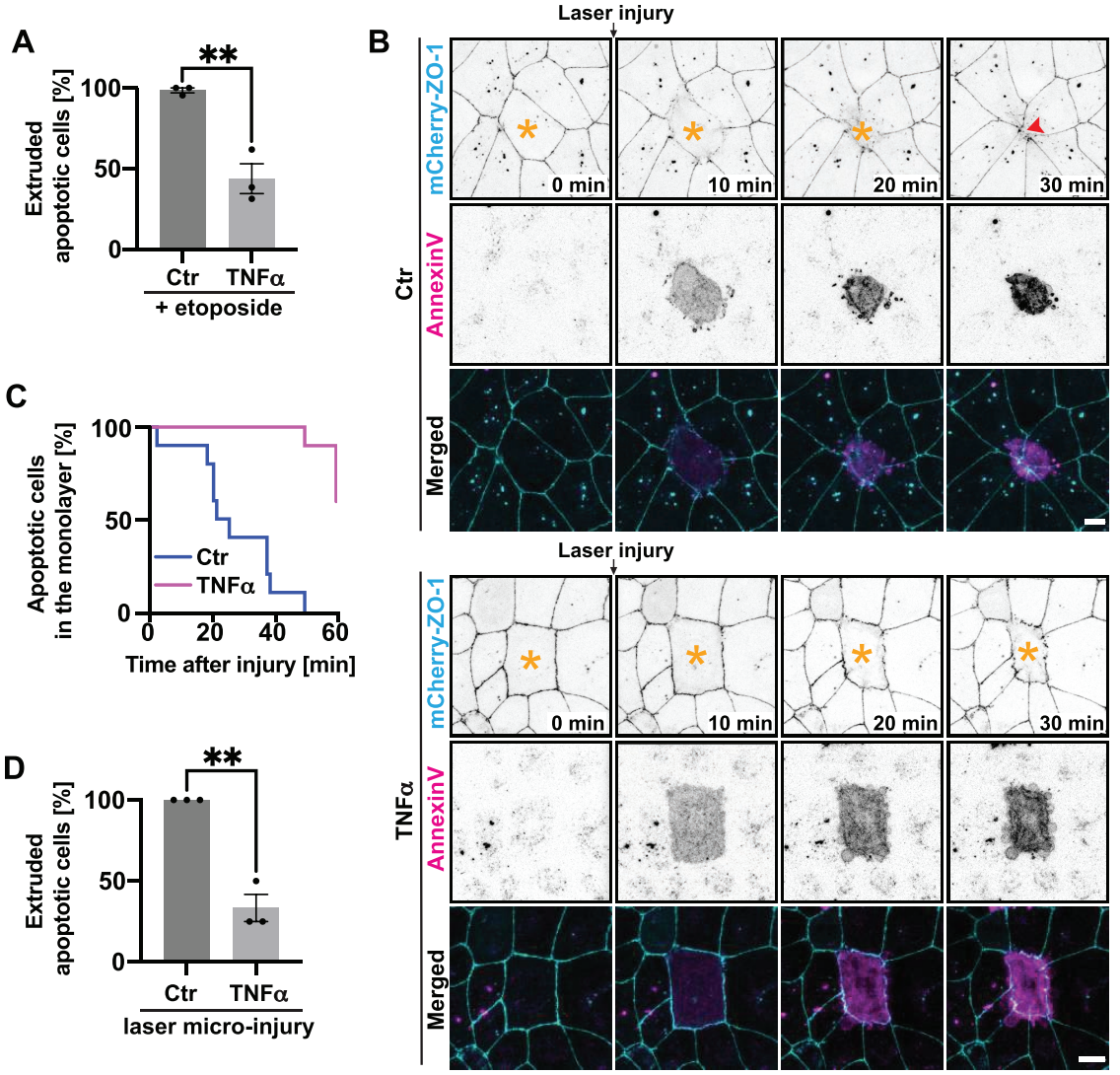

FIGURE 4: TNFα impairs apoptotic extrusion. (A) Quantification of extrusion efficiency in control and TNFα-treated cell lines. Apoptosis was induced by etoposide treatment (500 μM, 8 h). Apoptotic cells were detected using cleaved caspase-3 staining. (B–D) Selected frames from live imaging of 2-photon laser-mediated apoptosis in control and TNFα- treated cell lines (B). Apoptosis was confirmed by positive AnnexinV staining. Asterisks – apoptotic cells in the monolayer; arrowhead – junctional closure underneath extruded apoptotic cell. (C) Representation of time [min] apoptotic cells is present within the monolayer before extrusion is completed. (D) Quantification of efficiency of apoptotic extrusion in control and TNFα-treated cell lines; extrusion was classified as successful if apoptotic cells were expelled from the monolayers within 60 min of the 2- photon laser microinjury. Scale bars: 15 μm. XY panels are maximum projection views of all z-stacks. All data are means ± SEM; $^{**}p < 0.01$ calculated from $n \geq 3$ independent experiments analyzed with unpaired Student's *t* test.

Concluding remarks

Together, our findings indicate that preexisting mechanical tension in epithelial monolayers can condition the efficacy of apical extrusion as a homeostatic process. Specifically, apoptotic extrusion was inhibited by baseline mechanical hypertension induced by manipulating Myosin II. Taken with earlier evidence that extrusion of oncogene-expressing cells is also affected (Teo *et al.*, 2020a), this suggests that preexisting mechanical hypertension may exert a more general effect on apical extrusion.

How epithelial hypertension inhibits apoptotic extrusion is an important question for the future. Several possibilities warrant consideration. Mechanical hypertension may prevent neighboring cells from relaxing their orthogonal junctions sufficiently to elongate and execute extrusion (Teo *et al.*, 2020b). Alternatively, increased junction tension may affect lamellipodial crawling of neighboring cells, which has been suggested to drive extrusion in less confluent monolayers (Kocgozlu *et al.*, 2016) and helps seal the monolayer as apoptotic cells become expelled by purse-string contractility (Le *et al.*, 2021). As tissue mechanics can also affect cell signaling (Munjal *et al.*, 2015; Priya *et al.*, 2015), it is possible that mechanical hypertension influences pathways that allow an epithelial neighborhood response to the presence of apoptotic cells. For example, local activation of Erk1/2 and Akt has been demonstrated to modulate the local distribution of apoptosis and prevent cell injury from extending beyond apoptotic clusters (Gagliardi *et al.*, 2021; Valon *et al.*, 2021). It should also be noted that the MRLC-DD Myosin mutant used in our study may not reproduce contractile pulsatility, which is important for myosin-driven morphogenetic events such as

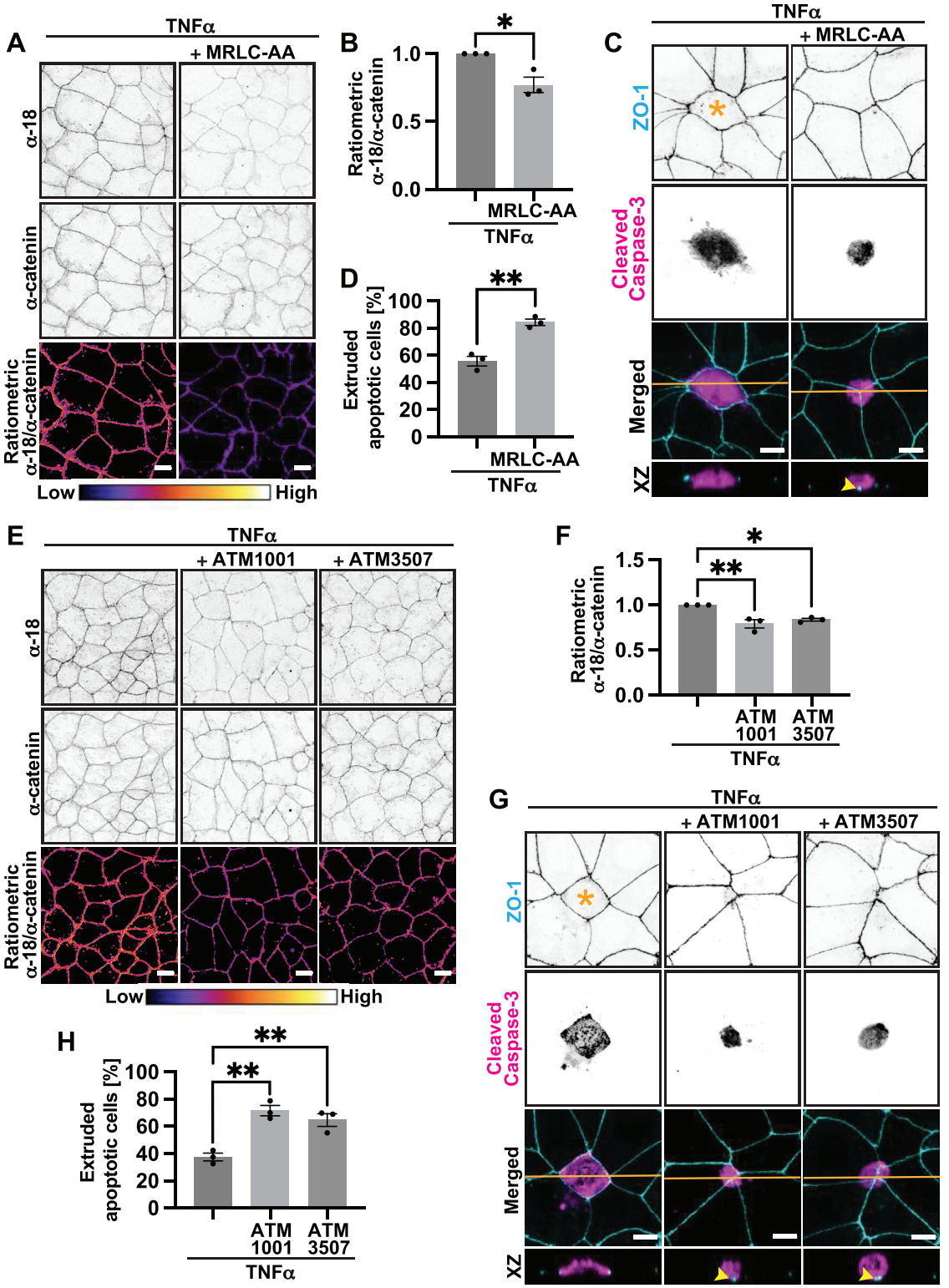

FIGURE 5: Correction of mechanical hypertension rescues apoptotic extrusion in TNFα–treated monolayers. (A and B) Representative images (A) and quantification (B) of junctional localization of α-catenin in open conformation (α-18) and total α-catenin in TNFα-treated cell lines upon expression of MRLC-AA. Ratiometric images represent junctional intensity of α-18 divided by junctional intensity of total α- catenin. (C and D) Representative images (C) and quantification (D) of extrusion efficiency in TNFα-treated cells upon expression of MRLC-AA. Apoptosis was inducted by etoposide treatment (500 μM, 8 h). Orange lines - location of the XZ views; asterisk – retained apoptotic cell; arrowhead – junctional closure underneath the extruded apoptotic cells. (E and F) Representative images (E) and quantification (F) of junctional localization of α-catenin in open conformation (α-18) and total α-catenin in TNFα stimulated cell lines upon treatment with tropomyosin inhibitors ATM1001 (2.5 μM, 8 h) and ATM3507 (2.5 μM, 8 h). Ratiometric images represent junctional intensity of α-18 divided by junctional intensity of total α-catenin. (G and H) Representative images (G) and

apical constriction (Vasquez *et al.*, 2016) and germband extension in Drosophila (Munjal *et al.*, 2015).

Finally, it is noteworthy that TNFα compromised apoptotic extrusion by inducing junctional hypertension. This carries the implication that pathogenetic factors, such as inflammatory cytokines, may exert some of their effects by altering tissue mechanics. Although TNFα induces apoptosis in some cells, this did not appear to be the case in our studies. The observed increase in number of apoptotic cells within monolayers was due to a failure of extrusion. Whether this might apply in other contexts is an interesting question for the future. Furthermore, while apoptosis is widely regarded as an immunologically silent phenomenon, we have recently reported that epithelia activate an acute, IL-8 driven, inflammatory response when apical extrusion fails to eliminate apoptotic cells (Duszyc *et al.*, 2023). This raises the interesting question of whether mechanical hypertension may increase the risk of provoking overt inflammation by blocking extrusion and causing apoptotic cells to be retained in epithelia.

MATERIALS AND METHODS

Request a protocol through *Bio-protocol*.

Cell lines and culture

Caco-2 and HEK-293T cells were cultured in RPMI and DMEM media, respectively, supplemented with 10% vol/vol Fetal Bovine Serum, 1% nonessential amino acids (NEAA), 1% L-glutamine, 100 U/ml Penicillin/Streptomycin and grown at 37°C in 5% CO_2 atmosphere. To produce lentivirus particles, required pLL5.0 expression vectors and packaging vectors were transfected into HEK-293T cells using Lipofectamine 2000 (Invitrogen). Twenty-four hours after transfection cell medium was changed to fresh DMEM supplemented with 10% serum, 1% NEAA and 1% L-glutamine. Forty-eight hours later virus containing medium was collected, filtered through a 0.45-µm syringe-driven filters and subsequently concentrated on Amicon Ultra-15 Centrifugal Filter Unit (Millipore, catalogue#UFC910096). Concentrated media containing lentiviral particles was used for infection of Caco-2 cells.

Antibodies

Primary antibodies used in this study were as follows-Rabbit pAb against Vinculin (Abcam, Catalogue#ab91459; RRID: AB_2050446)

Mouse mAb against α-catenin (Invitrogen, Catalogue# α-CAT-7A4; RRID: AB_2533044)

Rat pAb against α-18 (a kind gift from Akira Nagafuchi, Nara Medical University, Japan)

Rabbit mAb against Cleaved caspase-3 (Cell Signalling Technologies, Catalogue#9664; RRID: AB_2070042) Mouse mAb against ZO-1 (Invitrogen, Catalogue#33-9100; RRID: AB_2533147)

Mouse mAb against nonmuscle Myosin IIA (Abcam, Catalogue#ab55456; RRID: AB_944320)

Rabbit mAb against nonmuscle Myosin IIB (Biolegend, Catalogue#909901; RRID: AB_2565101)

Rabbit mAb against GAPDH (Abcam, Catalogue#ab181603; RRID: AB_2687666) Mouse mAb against β-Tubulin (Catalogue#T4026; RRID: AB_477577)

Mouse mAb against GFP (Sigma, Catalogue#11814460001 Roche; RRID: AB_390913)

Rat mAb against E-cadherin ectodomain (Invitrogen, Catalogue#13-1900; RRID: AB_2533005)

Alexa Fluor 647 Phalloidin (Invitrogen, Catalogue#A22287; RRID: AB_2621055)

Secondary antibodies were species-specific conjugated with AlexaFluor- 488, 546, 594, or 647 (Invitrogen) for immunofluorescence, or with horseradish peroxidase (Bio-Rad Laboratories) for immunoblotting.

TNFα and ATM1001/ATM3507 treatment

TNFα/IFN-γ treatment: Control and MRLC-AA–mutant Caco-2 cells were grown on glass coverslips or glass-bottom imaging dishes. Upon reaching 60–70% confluency, cells were treated with 10 ng/ml TNFα (R&D Systems, Catalogue#210-TA) and 10 ng/ml Interferon-γ (IFN-γ; Sigma, Catalogue#I3275) for 24 h.

ATM1001/ATM3507 treatment: Following 24 h of TNFα/IFN-γ treatment, cell media was supplemented with tropomyosin inhibitors ATM1001 (2.5 µM, 8 h) or ATM3507 (2.5 µM, 8 h), ± etoposide (500 µM, 8 h; Currier *et al.*, 2017; Kee *et al.*, 2018).

Immunostaining

Caco-2 cells were grown on glass coverslips until they reached 90–100% confluency. The cells were then fixed with 4% paraformaldehyde (PFA, 20 min, RT; Electron Microscopy Sciences, Catalogue#15710) prepared in cytoskeletal stabilization buffer (10 mM PIPES (piperazine-1,4-bis(2-ethanesulfonic acid), pH 6.8, 100 mM KCl, 300 mM sucrose, 2 mM EGTA (ethylene glycol tetraacetic acid), 2 mM $MgCl_2$). This was followed by a 5-min permeabilization with 0.25% Triton X-100. For vinculin immunostaining, cells were first prepermeabilized with an ice-cold permeabilization buffer (0.5% TritonX-100, 10 mM PIPES, 50 mM NaCl, 3 mM $MgCl_2$, 300 mM sucrose and 1X protease inhibitor) for 5 min on ice, and, thereafter, fixed with ice-cold 50% methanol diluted with acetone (1:1). Fixation was followed by blocking (1 h, RT) with 3% bovine serum albumin (BSA/0.01% Tween20/ phosphate-buffered saline [PBS]; Sigma, Catalogue#A-7906). Samples were incubated with primary antibodies (overnight, 4°C). Next, the coverslips were washed with 0.01% Tween20/PBS, followed by incubation with secondary antibody (1 h, RT). Coverslips were subsequently washed with 0.01% Tween20/ PBS and mounted with Prolong Gold Antifade reagent with DAPI (Cell Signalling Technologies, Catalogue#8961).

Microscopy and image analysis

Images of fixed samples were acquired using Zeiss LSM710 confocal microscope (40× oil objective with 1.3 N.A., 1 µm Z-slicing) driven by ZEN software. For quantification of junctional protein intensity, junctional immunofluorescence intensity was measured according to corrected total cell fluorescence (CTCF) analysis in ImageJ. Briefly, a segmented line of 5–10 pixel width was drawn parallelly over the junction, and its integrated density and area were measured. Then, the line was moved on either side of the junction to measure the background mean fluorescence. Next, CTCF was measured through the formula CTCF = integrated density – (area of

quantification (H) of extrusion efficiency in TNFα-stimulated cells upon treatment with tropomyosin inhibitors ATM1001 (2.5 µM, 8 h) and ATM3507 (2.5 µM, 8 h). Apoptosis was inducted by etoposide treatment (500 µM, 8 h). Orange lines - location of the XZ views; asterisk – retained apoptotic cell; arrowheads – junctional closure underneath the extruded apoptotic cells. Scale bars: 15 µm. XY panels are maximum projection views of all z-stacks. All data are means ± SEM; *$p < 0.05$, **$p < 0.01$, calculated from $n \geq 3$ independent experiments analyzed with unpaired Student's *t* test (B and D) or one-way ANOVA (F and H).

selected junction x average of background mean fluorescence). For each biological sample, a minimum of 50 junctions were analyzed across at least three independent repeats and the average junctional intensity was normalized to the control to compare fold-change across the groups.

Ratiometric vinculin/α-catenin and α-18/α-catenin image processing

To obtain ratiometric images of vinculin/α-catenin and α-18/total α-catenin staining, images were opened in Fiji and max projected (Image → Stacks → Z-project… → Projection type: Max Intensity). α- catenin channel was then processed using Gaussian Blur filter (Process → Filters → Gaussian Blur… → Sigma (Radius): 1) and thresholded to obtain junctional fraction of the staining. Junctional fraction was then selected (Edit → Selection → Create Selection → Make Inverse) and added to ROI. Obtained ROI was then applied to the max projected channels; nonselected space was filled with black color. Obtained junctional image fractions were then divided (Process → Image Calculator…) creating a 32-bit result ratiometric image, which was then presented as Fire LUT.

Immunoblotting

Cells were lysed in 1X lysis buffer (50mN Tris-HCl, 10% glycerol, 2% sodium dodecyl sulfate [SDS] and 0.1% Bromophenol Blue; 98°C, 10 min). The cell lysates were resolved in 12 or 14% SDS polyacrylamide gels, followed by transfer to nitrocellulose membrane and blocked with 5% nonfat milk in 0.01% Tween20/ Tris-buffered saline (TBS; 1 h, RT). The membranes were incubated with primary antibodies diluted in 3% BSA/0.01% Tween20/TBS (overnight, 4°C). Thereafter, the membranes were washed with 0.01% Tween20/TBS and incubated with the respective horse radish peroxidase -conjugated secondary antibody diluted in 3% BSA/0.01% Tween20/TBS (1 h, RT). The blots were visualized with Supersignal West Pico PLUS Chemiluminescent Substrate (ThermoFisher Scientific #34579) and imaged on Bio-Rad Chemidoc.

Junctional laser ablation

ZO-1-mCherry–tagged MRLC-DD mutant and control Caco-2 cells were cultured up to 90–100% confluency in 35-mm glass-bottom dishes. Imaging was performed on Zeiss LSM710 confocal microscope (63× oil objective with 1.4 N.A., 3× zoom, 1-μm Z-slicing) equipped with 2-photon fully tunable MaiTai eHP DeepSee 760–1040-nm laser and a 37°C heating chamber. An ablation ROI, sized 8 × 30 pixel, was positioned perpendicular to the longer axis of the ZO-1 marked junction. Following acquisition of a first frame, the ROI was ablated using 790 nm 2-photon laser at 30–40% transmission power for 10 iterations. Subsequent recoil of the cut junction was recorded for up to 1 min with 2 s frame intervals.

To analyze the recoil, the distance *(l)* between the vertices of the ablated junction was tracked in ImageJ with the MTrackerJ plugin and measured as a function of time *(t)*. Each junction was modelled as Kelvin-Voigt fiber and mean values of tracked distances before and after laser ablation (*l[0]* and *l[t]*, respectively) were plotted against time, and calculated by nonlinear regression of the data to the following equation -

$$f(t) = l(t) - l(0) = \frac{A}{k} \cdot \left(1 - e^{-kt}\right)$$

where *l(t)* is defined as the distance between the two vertices at any time point *t*, *A* is the initial recoil indicating the tensile force at the junction before laser ablation, and *k* is the viscosity coefficient assumed to be constant and calculated as –

$$k = \frac{E}{\mu}$$

Where *E* is the elastic modulus of the junction, and μ is the viscosity coefficient related to viscous drag of the media. *k* values not changing significantly reflect that the initial recoil of the junction is a feature of changes in tensile force alone.

Etoposide-induced apoptosis

Caco-2 cells were grown on glass coverslips up to 90–100% confluency and were then treated with 500 μM etoposide (AdooQ Bioscience, Catalogue#A10373) for 8 h at 37°C. After treatment, cells were fixed with 100% ice-cold methanol for 10 min and immunostained for junctional marker ZO-1, apoptotic cell marker cleaved caspase-3 and nuclear stain DAPI.

Laser injury induced cell injury

Laser-induced cell injury was performed on Zeiss LSM710 confocal microscope equipped with the 2- photon fully tunable MaiTai eHP DeepSee 760–1040-nm laser and a 37°C heating chamber. Caco-2 cells were cultured up to 90–100% confluency in 35-mm glass-bottom dishes. To induce apoptosis, nuclear microirradiation was performed using 10 iterations of 790 nm 2-photon laser at 50–70% transmission power (63× oil objective with 1.4 N.A., 1 μm Z-slicing). To confirm successful induction of apoptosis, cell media was supplemented with an apoptotic detection marker AnnexinV (Invitrogen, Catalogue#A23204).

TET-Inducible Puma

Double-positive MRLC-DD^{PUMA} or Control^{PUMA} cells were seeded with MRLC-DD and control GFP Caco- 2 cells in a 1:100 ratio onto glass coverslips. Once confluent, the cocultures were treated with 2 μg/ml doxycycline (Sigma, Catalogue#D9891) to initiate apoptosis in the Puma cells. Cells were fixed at 4-, 6-, and 8-h time-points and were immunostained for apoptotic marker cleaved caspase-3 and nuclear stain DAPI.

Quantification of apoptotic extrusion

Etoposide-induced apoptosis: Extrusion was considered 1) successful if an apoptotic, cleaved caspase-3 positive cell was located above the apical plane of the monolayer (as indicated by the ZO-1 staining); (2) failed if an apoptotic, cleaved caspase-3 positive cell was located within the same z-plane as the neighbors in monolayer. Extrusion efficiency is presented as a percentage of successfully extruded apoptotic cells.

Laser-induced apoptosis: Extrusion was considered 1) successful if an injured cell stained positive for apoptotic marker AnnexinV (Invitrogen, Catalogue#A23204) and was apically expelled from the monolayer (as indicated by the ZO-1-tagged neighbour cells' rosette formation underneath the injured cell) within 60 min of laser injury; 2) failed if 60 min after the laser injury, apoptotic cell was still located within the monolayer, at the same plane as the neighboring cells. Extrusion efficiency is presented as a percentage of successfully extruded apoptotic cells.

Puma-induced apoptosis: Only apoptotic, cleaved caspase-3 positive PUMA cells were included in the quantification. Extrusion was considered 1) successful if the nucleus of an apoptotic, mCherry-positive PUMA cell was located at a z-plane above the nuclei of the surrounding cells; 2) failed if the nucleus of an apoptotic, mCherry-positive PUMA cell was located at the same z-plane as the nuclei of the surrounding cells. Extrusion efficiency is presented as a percentage of successfully extruded apoptotic PUMA-positive cells.

Quantification of apoptotic rates

Preparation of samples for immunoblotting: Confluent Caco-2 cells were treated with 500 μM etoposide (AdooQ Bioscience, Catalogue#A10373; 24 h, 37°C). Following the treatment, cell media was collected and spun down (2000 rpm, 3 min). Supernatant was discarded, while the pellet containing extruded apoptotic cells was combined with cells scraped from the respective experimental dish. Cells were lysed in 1X lysis buffer (50mN Tris-HCl, 10% glycerol, 2% SDS and 0.1% Bromophenol Blue; 98°C, 10 min) and used for immunoblotting as described above.

Live-imaging: Confluent Caco-2 cells were imaged on Zeiss LSM710 confocal microscope (20× dry objective with 0.8 N.A., 2 μm Z-slicing). Imagining media was supplemented with 5 μM CellEvent Caspase-3/7 Detection Regent (Invitrogen, Catalogue#C10423) and, if required, 500 μM etoposide (AdooQ Bioscience, Catalogue#A10373). Imaging was carried out for 16 h with 10 min/frame imaging frequency. Any cell that stained positive with CellEvent Caspase-3/7 reagent was recorded as an apoptotic cell, regardless of the cell position within the monolayer/extrusion state.

Statistics

All graphs represented are the mean ± SEM from at least three independent repeats. Statistical analyses were performed using GraphPad Prism 9, to obtain *p* values with 95% confidence intervals. Unpaired student's *t* test was used to compare datasets between two groups, and either one-way or two-way ANOVA used to compare three or more groups, depending on the number of variables.

ACKNOWLEDGMENTS

We thank our colleagues for their support and advice throughout this project. Our work was supported by grants from the National Health and Medical Research Council of Australia (1136592 and 1163462 to A.S.Y; 1079866 and 1100202 to P.W.G and E.C.H); the Australian Research Council (DP220103951 to A.S.Y); Australian Department of Industry, Science and Resources (CRC-P-355 to P.W.G and E.C.H); and by the US Department of Defense (Discovery Grant HT94252310088 to A.S.Y, J.B and J.M.D). Microscopy was performed at the ACRF/IMB Cancer Research Imaging Facility created with the generous support of the Australian Cancer Research Foundation. Additionally, we acknowledge support from the NCCS Bioimaging Centre.

REFERENCES

Andrade D, Rosenblatt J (2011). Apoptotic regulation of epithelial cellular extrusion. Apoptosis 16, 491–501.

Atieh Y, Ruiz OE, Eisenhoffer GT (2021). Protocol for quantitative analysis of pulsatile contractions and cell extrusion in epithelial tissues of larval zebrafish. STAR Protoc 2, 100600. https://doi.org/10.1016/j.xpro.2021.100600

Bonfim-Melo A, Noordstra I, Gupta S, Chan AH, Jones MJK, Schroder K, Yap AS (2022). Rapid lamellipodial responses by neighbor cells drive epithelial sealing in response to pyroptotic cell death. Cell Rep 38, 110316.

Bradley JR (2008). TNF-mediated inflammatory disease. J Pathol 214, 149–160.

Caldwell BJ, Lucas C, Kee AJ, Gaus K, Gunning PW, Hardeman EC, Yap AS, Gomez GA (2014). Tropomyosin isoforms support actomyosin biogenesis to generate contractile tension at the epithelial zonula adherens. Cytoskeleton (Hoboken) 71, 663–676.

Charras G, Yap AS (2018). Tensile forces and mechanotransduction at cell-cell junctions. Curr Biol 28, R445–R457.

Curran S, Strandkvist C, Bathmann J, de Gennes M, Kabla A, Salbreux G, Baum B (2017). Myosin II controls junction fluctuations to guide epithelial tissue ordering. Dev Cell 43, 480–492 e486.

Currier MA, Stehn JR, Swain A, Chen D, Hook J, Eiffe E, Heaton A, Brown D, Nartker BA, Eaves DW, *et al*. (2017). Identification of cancer-targeted tropomyosin inhibitors and their synergy with microtubule drugs. Mol Cancer Ther 16, 1555–1565.

Duszyc K, Gomez GA, Lagendijk AK, Yau MK, Nanavati BN, Gliddon BL, Hall TE, Verma S, Hogan BM, Pitson SM, *et al*. (2021a). Mechanotransduction activates RhoA in the neighbors of apoptotic epithelial cells to engage apical extrusion. Curr Biol 31, 1326–1336 e1325.

Duszyc K, Noordstra I, Yap AS, Gomez GA (2021b). Live imaging of apoptotic extrusion and quantification of apical extrusion in epithelial cells. Bio Protoc 11, e4232.

Duszyc K, von Pein JB, Ramnath D, Currin-Ross D, Verma S, Lim F, Sweet MJ, Schroder K, Yap AS (2023). Apical extrusion prevents apoptosis from activating an acute inflammatory program in epithelia. Dev Cell 58, 2235–2248.e6.

Gagliardi PA, Dobrzynski M, Jacques MA, Dessauges C, Ender P, Blum Y, Hughes RM, Cohen AR, Pertz O (2021). Collective ERK/Akt activity waves orchestrate epithelial homeostasis by driving apoptosis-induced survival. Dev Cell 56, 1712–1726 e1716.

Gough P, Myles IA (2020). Tumor necrosis factor receptors: pleiotropic signaling complexes and their differential effects. Front Immunol 11, 585880.

Graham WV, Wang F, Clayburgh DR, Cheng JX, Yoon B, Wang Y, Lin A, Turner JR (2006). Tumor necrosis factor-induced long myosin light chain kinase transcription is regulated by differentiation-dependent signaling events. Characterization of the human long myosin light chain kinase promoter. J Biol Chem 281, 26205–26215.

Heer NC, Martin AC (2017). Tension, contraction and tissue morphogenesis. Development 144, 4249–4260.

Jang DI, Lee AH, Shin HY, Song HR, Park JH, Kang TB, Lee SR, Yang SH (2021). The role of tumor necrosis factor alpha (TNF-alpha) in autoimmune disease and current TNF-alpha inhibitors in therapeutics. Int J Mol Sci 22, 2719.

Kee AJ, Chagan J, Chan JY, Bryce NS, Lucas CA, Zeng J, Hook J, Treutlein H, Laybutt DR, Stehn JR, *et al*. (2018). On-target action of anti-tropomyosin drugs regulates glucose metabolism. Sci Rep 8, 4604.

Kocgozlu L, Saw TB, Le AP, Yow I, Shagirov M, Wong E, Mege RM, Lim CT, Toyama Y, Ladoux B (2016). Epithelial cell packing induces distinct modes of cell extrusions. Curr Biol 26, 2942–2950.

Le AP, Rupprecht JF, Mege RM, Toyama Y, Lim CT, Ladoux B (2021). Adhesion-mediated heterogeneous actin organization governs apoptotic cell extrusion. Nat Commun 12, 397.

Lecuit T, Yap AS (2015). E-cadherin junctions as active mechanical integrators in tissue dynamics. Nat Cell Biol 17, 533–539.

Leppkes M, Roulis M, Neurath MF, Kollias G, Becker C (2014). Pleiotropic functions of TNF-alpha in the regulation of the intestinal epithelial response to inflammation. Int Immunol 26, 509–515.

Liang X, Michael M, Gomez GA (2016). Measurement of mechanical tension at cell-cell junctions using two-photon laser ablation. Bio Protoc 6, e2068.

Lubkov V, Bar-Sagi D (2014). E-cadherin-mediated cell coupling is required for apoptotic cell extrusion. Curr Biol 24, 868–874.

Ma TY, Boivin MA, Ye D, Pedram A, Said HM (2005). Mechanism of TNF-alpha modulation of Caco-2 intestinal epithelial tight junction barrier: role of myosin light-chain kinase protein expression. Am J Physiol Gastrointest Liver Physiol 288, G422–430.

Michael M, Meiring JCM, Acharya BR, Matthews DR, Verma S, Han SP, Hill MM, Parton RG, Gomez GA, Yap AS (2016). Coronin 1B reorganizes the architecture of F-Actin networks for contractility at steady-state and apoptotic adherens junctions. Dev Cell 37, 58–71.

Micheau O, Tschopp J (2003). Induction of TNF receptor I-mediated apoptosis via two sequential signaling complexes. Cell 114, 181–190.

Munjal A, Philippe JM, Munro E, Lecuit T (2015). A self-organized biomechanical network drives shape changes during tissue morphogenesis. Nature 524, 351–355.

Nagafuchi A, Tsukita S (1994). The loss of the expression of alpha catenin, the 102 kD cadherin associated protein, in central nervous tissues during development: (alpha catenin/cadherin/cell adhesion/CNS). Dev Growth Differ 36, 59–71.

Noordstra I, Morris RG, Yap AS (2023). Cadherins and the cortex: A matter of time? Curr Opin Cell Biol 80, 102154.

Priya R, Gomez GA, Budnar S, Verma S, Cox HL, Hamilton NA, Yap AS (2015). Feedback regulation through myosin II confers robustness on RhoA signalling at E-cadherin junctions. Nat Cell Biol 17, 1282–1293.

Reindl T, Giese S, Greve JN, Reinke PY, Chizhov I, Latham SL, Mulvihill DP, Taft MH, Manstein DJ (2022). Distinct actin-tropomyosin cofilament populations drive the functional diversification of cytoskeletal myosin motor complexes. iScience 25, 104484.

Rosenblatt J, Raff MC, Cramer LP (2001). An epithelial cell destined for apoptosis signals its neighbors to extrude it by an actin- and myosin-dependent mechanism. Curr Biol 11, 1847–1857.
Ruder B, Atreya R, Becker C (2019). Tumour necrosis factor alpha in intestinal homeostasis and gut related diseases. Int J Mol Sci 20, 1887.
Teo JL, Gomez GA, Weeratunga S, Davies EM, Noordstra I, Budnar S, Katsuno-Kambe H, McGrath MJ, Verma S, Tomatis V, *et al*. (2020a). Caveolae control contractile tension for epithelia to eliminate tumor cells. Dev Cell 54, 75–91 e77.
Teo JL, Tomatis VM, Coburn L, Lagendijk AK, Schouwenaar IM, Budnar S, Hall TE, Verma S, McLachlan RW, Hogan BM, *et al*. (2020b). Src kinases relax adherens junctions between the neighbors of apoptotic cells to permit apical extrusion. Mol Biol Cell 31, 2557–2569.
Tracey KJ, Cerami A (1994). Tumor necrosis factor: A pleiotropic cytokine and therapuetic target. Annu Rev Med 45, 491–503.
Valon L, Davidovic A, Levillayer F, Villars A, Chouly M, Cerqueira-Campos F, Levayer R (2021). Robustness of epithelial sealing is an emerging property of local ERK feedback driven by cell elimination. Dev Cell 56, 1700–1711 e1708.
Vasquez CG, Heissler SM, Billington N, Sellers JR, Martin AC (2016). Drosophila non-muscle myosin II motor activity determines the rate of tissue folding. eLife 5, e20828.
Wang D, Wang Y, Di X, Hardeman EC, Jin D, Gunning PW (2023). Cortical tension drug screen links mitotic spindle integrity to Rho pathway. Curr Biol 33, 1–12.
Yao M, Qiu W, Liu R, Efremov AK, Cong P, Seddiki R, Payre M, Lim CT, Ladoux B, Mege RM, Yan J (2014). Force-dependent conformational switch of alpha-catenin controls vinculin binding. Nat Commun 5, 4525.
Yonemura S, Wada Y, Watanabe T, Nagafuchi A, Shibata M (2010). alpha-Catenin as a tension transducer that induces adherens junction development. Nat Cell Biol 12, 533–542.